X-Ray Diffraction Study of the Electron Density and Anharmonicity in K_2PtCl_6 *

Renzo Restori and Dieter Schwarzenbach

Institute of Crystallography, University of Lausanne, BSP, CH-1015 Lausanne, Switzerland

Z. Naturforsch. **48a**, 12–20 (1993); received December 19, 1991

X-ray diffraction data in heavy-atom compounds may be sensitive to anharmonic atomic displacements, since the large core electron densities result in appreciable scattering amplitudes at large reciprocal distances. Since bonding electron densities may also exhibit sharp features affecting high-order reflections, they may be difficult to distinguish from anharmonic effects. We have analyzed an accurate room-temperature single-crystal X-ray data set of K_2PtCl_6 using least-squares anharmonic displacement and charge density formalisms. The Hirshfeld charge density formalism, which has successfully been applied to many light-atom structures, fails to parametrize satisfactorily the data, whereas the electron densities at K and Cl are easily accounted for by an anharmonic Gram-Charlier expansion to 4th order. Densities around Pt are parametrized only by a combination of anharmonicity and charge density formalisms. If economical parametrizations of the experimental data are preferred to more complicated ones, anharmonicity may be conjectured to play an important rôle while the main bonding feature consists of a preferential occupation of the 5d-orbitals of Pt with t_{2g} symmetry.

Key words: Charge density; Thermal motion; Anharmonicity; X-ray diffraction; d-orbitals.

Introduction

In a single X-ray diffraction experiment it is not possible to distinguish unambiguously between bonding effects and vibrational smearing of the electron density in a crystal [1]. In the absence of supplementary evidence, as e.g. neutron diffraction data or diffraction experiments carried out at different temperatures, the two properties are distinguished indirectly by assuming that they affect Bragg intensities essentially in more or less distinct ($\sin\theta/\lambda$)-ranges. Thus, structure amplitudes at large reciprocal distances should give information mainly on the atomic coordinates and thermal displacement parameters, whereas low-order reflections should carry more information on chemical bonding. In fact, correlations encountered in least-squares calculations between standard parameters of the spherical-atom (*procrystal*) model and electron density parameters usually decrease if high-order data are available. However, sharp bonding density features may scatter very far out into reciprocal space and become essentially indistinguishable with harmonic and/or anharmonic displacement parameters.

This problem may become particularly important in the case of heavy atoms. On the one hand, the features attributed to the occupation of d-orbitals in transition-metal compounds have been described as peaking sharply at only 0.3 to 0.4 Å from the atomic center [2–4]. On the other hand, electron densities at the centres of heavy atoms are very large, as evidenced by the correspondingly large values of the atomic form factors at large $\sin\theta/\lambda$. High-order Bragg intensities are therefore easily observable and may be more sensitive to contributions from anharmonic displacements than are neutron data. Minima of the non-spherical bonding features around transition metal centres tend to be located in the directions of the nearest-neighbour atoms, whereas the maxima lie between metal-ligand bonds and thus point toward second-nearest neighbours [2–4]. Anharmonic motions would be expected to have smaller amplitudes towards nearest neighbours and larger amplitudes towards second-nearest neighbours or structural voids; they would thus be expected to create much the same type of electron density features as the d-electron distribution.

In this paper, we report an accurate X-ray diffraction study of K_2PtCl_6 at room temperature, compris-

* Presented at the Sagamore X Conference on Charge, Spin and Momentum Densities, Konstanz, Fed. Rep. of Germany, September 1–7, 1991.

Reprint requests to Prof. Dr. D. Schwarzenbach, Institut de Cristallographie, BSP, Université de Lausanne, CH-1015 Lausanne, Schweiz/Suisse.

0932-0784 / 93 / 0100-0012 $ 01.30/0. – Please order a reprint rather than making your own copy.

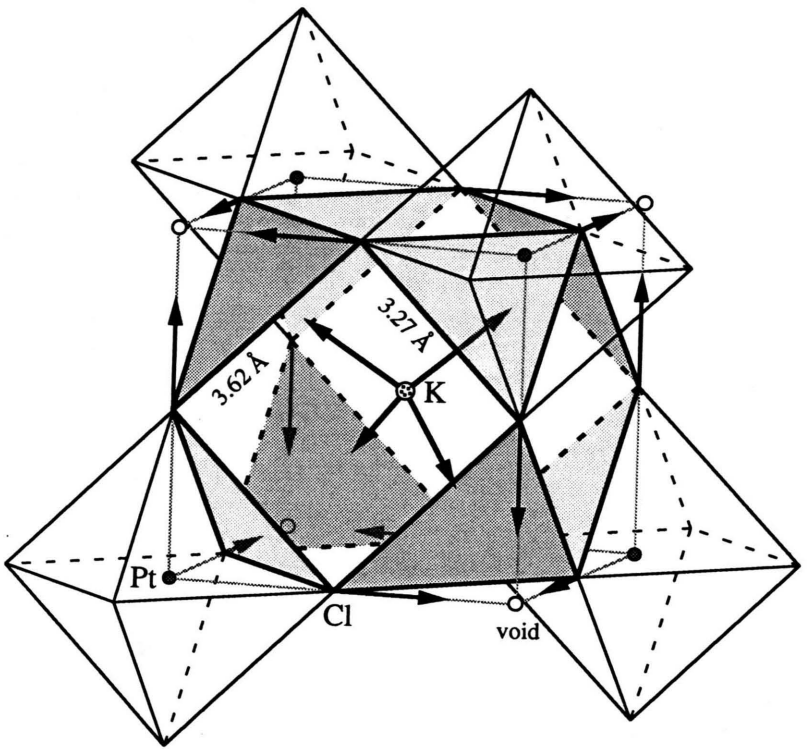

Fig. 1. Coordination polyhedra in K_2PtCl_6. The arrows point to the unoccupied Cl_6-octahedral voids; they also represent the directions of largest displacements in the anharmonic models.

ing various electron-density and anharmonic-motion refinements. This heavy-atom compound crystallizes in the cubic space group $Fm\bar{3}m$ with $Z=4$ formula units per cell, $a = 9.743(3)$ Å. Site symmetries are $m\bar{3}m$ for Pt at 0, 0, 0, $\bar{4}3m$ for K at 1/4, 1/4, 1/4 and 4mm for Cl at x, 0, 0 ($x \approx 0.237$). Pt is coordinated octahedrally by Cl. K is coordinated by 12 Cl on the corners of a distorted cuboctahedron with four large and four small triangular faces (Figure 1); located across the small faces are nearest-neighbour Pt-atoms, and across the large faces are non-occupied Cl_6-octahedral voids. Cl is also coordinated cuboctahedrally by 8 Cl and 4 K. The difference electron density distribution around Pt in K_2PtCl_6 as determined from X-ray data at 120 K [5] shows lobes of positive density directed towards the faces of the coordination octahedron. This feature has been attributed to filled 5d-orbitals with t_{2g} symmetry and empty 5d-orbitals with e_g symmetry, but anharmonic vibrations of Pt would be expected to create excess density in the same directions. Anharmonic motions of K and of Cl would be expected to create excess densities in the directions pointing towards the unoccupied octahedral voids and opposite to the nearest Pt-neighbours.

Experimental

Commerical K_2PtCl_6 was recrystallized from aqueous solution. A crystal possessing a nearly perfect octahedral shape {111} was chosen for data collection at room temperature on an Enraf-Nonius CAD-4 diffractometer using AgKα radiation ($\lambda_{\bar{\alpha}} = 0.56087$ Å) and a graphite (002) monochromator. Distances between parallel faces of the octahedron were measured with a telescope equipped with an eyepiece micrometer and mounted on the diffractometer; they were found to be equal within the estimated precision of 0.002 mm, their mean value being 0.0969 mm. Diffraction intensities were measured with 2θ-ω scans over a half-sphere in reciprocal space ($h > 0$) to $(\sin\theta/\lambda)_{max} = 1.3$ Å^{-1}. If necessary, measurements were repeated to ensure that each set of symmetry-equivalent reflections contained at least 12 observations. ω-scan speeds were 0.550°/min for $0 \leq \theta \leq 35°$, 0.275°/min for $35 \leq \theta \leq 40°$ and 0.166°/min for $40 \leq \theta \leq 47°$. The total ω-scan angle was 1.5 $(0.6 + 0.446 \tan\theta)°$; the first and last sixths of the scan were assumed to be background. The counter aperture width was 1.32° vertically and $(0.66 + 0.13 \tan\theta)°$ horizontally. Three intensity-control

reflections were measured every 3 hours. The resulting number of observations is 9007. Unweighted averaging of symmetry-equivalent absorption-corrected ($\mu = 9.549\ mm^{-1}$) data resulted in 489 inequivalent intensities. Corresponding standard deviations were obtained in the usual way using the deviations of individual intensities from the sample means[1]. The ratio of the average deviation and the average intensity was $R_{int} = 0.012$.

Least-squares Refinements

The charge density and anharmonic refinement program used in this work is described in [3]. In addition to the standard procrystal model defined by positional and anisotropic displacement parameters, scale factor and secondary extinction parameters [6], the program provides the Gram-Charlier expansion of anharmonic motion [7] up to 4th order, and a representation of the asphericity of the atoms by means of a sum of multipolar deformation functions $\varrho_{nlm\pm} = P_{nlm\pm} r^n \exp(-\alpha r) C_{lm\pm} y_{lm\pm}$ [8], which may be chosen to be equivalent to the deformation functions of Hirshfeld [9]. The terms $y_{lm\pm}$ are real spherical harmonic functions [10], the $C_{lm\pm}$ are their normalization constants, and r is the distance from the atomic center. For Pt and K, cubic spherical harmonics are defined by $y_{K3} = y_{32-}$, $y_{K4} = y_{40+} + y_{44+}/168$ [10]. The population factors $P_{nlm\pm}$ and the radial exponents α are adjustable parameters. The indices of the site-symmetric functions are:

- anharmonic parameters 1111, 1122 for Pt; 123, 1111, 1122 for K; 111, 122, 1111, 2222, 1122, 2233 for Cl;
- spherical harmonics $lm\pm = 00$, K4 for Pt; 00, K3, K4 for K; 00, 10, 20, 30, 40, 44+ for Cl [10].

All refinements were carried out with respect to $|F_o|^2$, including negative values [11], with weights equal to the inverse variances. An isotropic type I extinction model with Lorentzian mosaic distribution was included in all refinements. Smallest extinction factors y_{min} ($|F_{corr}| = y|F_o|$) were similar in all cases, viz. 0.81 for 400, 0.84 for 111 and 0.89 for 200. Convergence was considered complete if all ratios (full shift/standard deviation) $< 10^{-4}$.

[1] A list of mean absorption-corrected intensities and standard deviations can be obtained from D. Schwarzenbach.

Scattering factors in analytical form for neutral free atoms and dispersion corrections were taken from [12]. The following refinements were carried out:

S: Standard refinement of 7 variables, viz. a scale factor, an extinction parameter, a positional parameter x of Cl and 4 displacement parameters.

A: Anharmonic refinement comprising 7 standard and 11 additional displacement parameters.

B: Deformation density refinement equivalent to the Hirshfeld deformation model [9] comprising 7 standard and 22 deformation parameters ($n=0$, 2, 4 for $l=0$; $n=1$, 3 for $l=1$; $n=2$, 4 for $l=2$; $n=3$ for $l=3$; $n=4$ for $l=4$; 3 exponents α).

C: Deformation density refinement *more* flexible than the Hirshfeld model including, in addition to the functions used in *B*, an octupolar ($l=3$) function with $n=5$ on K and hexadecapolar ($l=4$) functions with $n=6$ on both K and Pt. The resulting number of deformation parameters is 25.

D: Deformation density refinement including the same functions as used in *C*. Two radial exponents α were refined for K and Cl, one for the monopolar ($l=0$) functions and one for all the other functions, increasing the number of deformation parameters to 27. Due to high correlations between the parameters, convergence of the least-squares procedure was difficult to attain; three of the 5 α-values did not stop oscillating at successive cycles using damping factors of 0.01 and were set to the corresponding mean values. Under these circumstances, refinement of two α-values for Pt was not attempted.

E: Combined anharmonic and deformation density refinement using the parameters of *A* and *B*, thus 7 standard and 33 additional variables.

F: Combined anharmonic and deformation density refinement with fewer variables than *E*, *including* an $n=5$ octupole on K and $n=6$ hexadecapoles on K and Pt as in *C*, and *excluding* all monopolar functions ($l=0$, $n=0$, 2, 4) of all atoms. Monopoles are thus taken care of by the 4th-order anharmonic terms. This results in 27 variables in addition to the 7 standard variables.

The resulting standard parameter values and reliability factors obtained in these refinements are reported in Table 1.

In order to check on the precision of the observed shape of the crystal, an additional refinement of the 7

Table 1. Standard parameters and agreement factors obtained with the refinements mentioned in the text. Positional (x) and displacement parameters (U) are multiplied by 10^5. The displacement factor expression is $\exp(-2\pi^2 a^{-2} \sum U_{ij} h_i h_j)$. Estimated standard deviations are given in parentheses. U_{par} and U_{perp} are parallel and perpendicular to the Pt–Cl bond ⟨100⟩, respectively; g_{ext} is the extinction coefficient; the goodness of fit is $S = \{\sum \text{weight}(|F_o|^2 - |F_c|^2)^2/(n-m)\}^{1/2}$, n = number of observations, m = number of variables; $wR(|F|^2) = \{\sum \text{weight}(|F_o|^2 - |F_c|)^2/\sum \text{weight}\,|F_o|^4\}^{1/2} \approx 2w\,R(|F|)$.

	S	*A*	*B*	*C*	*D*	*E*	*F*
Scale	2.944(1)	2.983(2)	2.724(14)	2.719(11)	2.697(14)	3.020(26)	2.983(2)
$10^4\,g_{ext}$	0.286(2)	0.321(2)	0.289(4)	0.286(4)	0.277(3)	0.316(10)	0.321(3)
U(Pt)	1465(1)	1559(3)	1376(4)	1371(4)	1366(4)	1196(97)	1558(4)
U(K)	3697(7)	3784(15)	3497(26)	3530(18)	3532(14)	3262(598)	3772(15)
x(Cl)	23743(2)	23719(3)	23747(3)	23746(3)	23933(41)	23724(5)	23719(6)
U_{par}(Cl)	1606(6)	1665(12)	1486(11)	1495(10)	478(137)	1751(41)	1719(18)
U_{perp}(Cl)	4168(7)	4342(16)	3977(13)	3969(12)	4394(56)	4385(48)	4290(19)
S	2.080	1.213	1.334	1.206	1.055	0.971	1.018
$wR(\|F\|^2)$	0.0157	0.0091	0.0099	0.0089	0.0078	0.0071	0.0075

standard parameters and parameters describing the crystal shape was carried out on the complete unaveraged data set that was corrected for Lorentz and polarization effects, but *not* for absorption. As has been proposed in [13] and [14], the observed distances of 0.0969 mm between opposite faces of the octahedron were introduced as restraints with minimum-variance weights $(0.002)^{-2}$. The refined distances are 0.0972, 0.0961, 0.0967, and 0.0938 mm, in excellent agreement with the observed values.

Difference-density and Residual Maps

All maps discussed in this section were computed with Fourier series. The *difference-density* maps show essentially the features parametrized by the respective anharmonic and deformation density models. The Fourier coefficients used for calcuating them are $(F_c - F_S)$, F_c being the calculated structure factor of the relevant refinement A to F, and F_S being the calculated structure factor of the standard refinement S. The sums include 1126 symmetry-independent terms calculated up to $(\sin\theta/\lambda)_{max} = 1.762$ Å^{-1}.

The *residual maps* show the features *not* parametrized by the respective anharmonic and deformation density models. The Fourier coefficients used for calculating them are $(\text{sign}_c\,|F_o| - F_c)$, where $|F_o|$ is the observed structure factor, F_C has the same meaning as above, and sign_c is the sign of F_c. The sums include all observed data.

Fig. 2 shows the residual map resulting from the standard refinement S. The density around K has positive lobes pointing towards the large triangles and

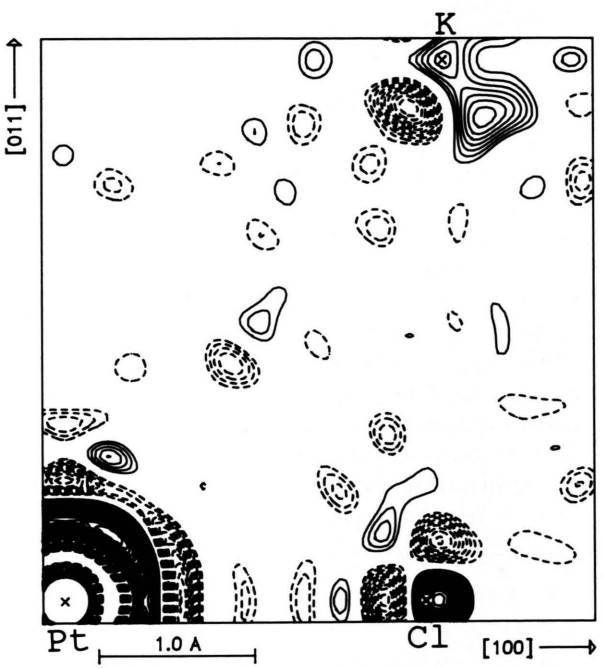

Fig. 2. Residual map of the standard refinement S in the plane $(0\bar{1}1)$. Contour intervals are 0.05 eÅ^{-3}, negative contours broken, contours with $|\varrho| \leq 0.1$ eÅ^{-3} omitted.

negative lobes pointing towards the small triangles of the coordinating cuboctahedron (Figure 1). Near Cl on the Pt–Cl bond, there is a depletion of density towards Pt and an accumulation of density away from Pt. The density at Pt is dominated by series-termination ripples whose zero contours at distances larger than $r = 0.75$ Å coincide with the zeros of the function $\Phi(x) = 3x^{-3}(\sin x - x\cos x)$, $x = 4\pi(\sin\theta/\lambda)_{max}\,r$. We

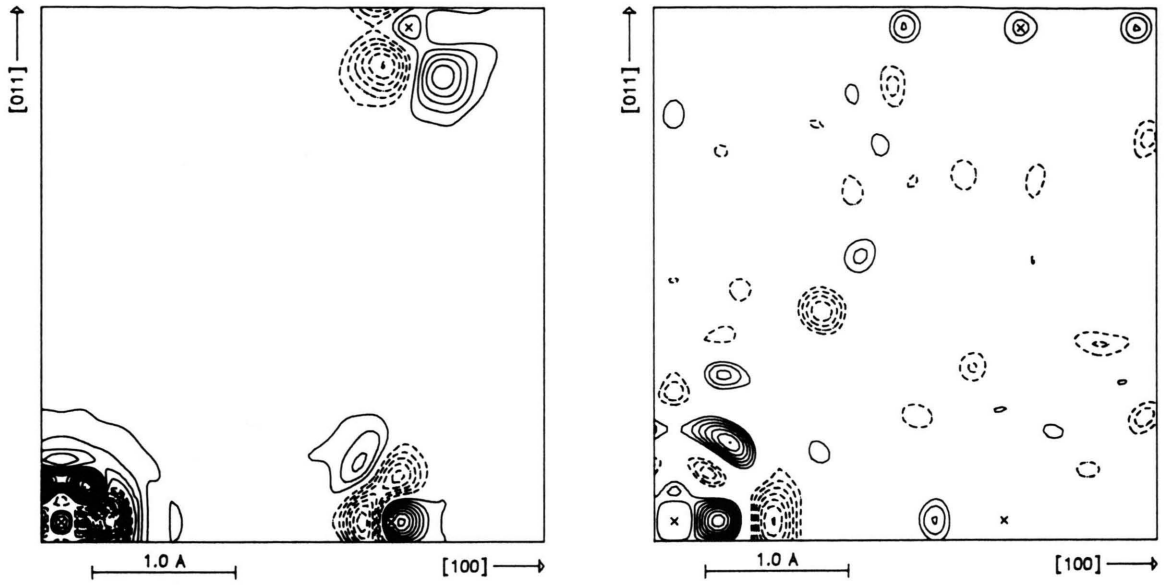

Fig. 3. Difference map (left) and residual map (right) of the anharmonic refinement *A*. Contour intervals are: in the difference map 0.10 eÅ^{-3} and $\varrho = 0$ omitted; in the residual map 0.05 eÅ^{-3} and $|\varrho| \leq 0.1$ eÅ^{-3} omitted; negative contours broken. Atomic site labels are given in Figure 2.

conclude that an important spherically-symmetric accumulation of density ϱ_{spher} on Pt is not taken care of by the standard refinement, the features around Pt representing mainly the convolution $\varrho_{\text{spher}} * \Phi$. The ripples appear also in all difference-density maps of refinements *A* to *F* with zeros corresponding to the higher resolution of these maps of $(\sin\theta/\lambda)_{\max} = 1.762$ Å^{-1}. In order to reveal the aspherical features, the spherical features were removed from all the difference density maps of Figs. 3–8 using the following functions chosen *empirically* by trial and error:

- centred on Pt, $c_{\text{Pt}}\Phi(x)$ with $x = 22.142\,r$, for subtracting the series termination ripples at distances $r \geq 0.75$ Å;
- centred on K and Cl, Lorentzian functions $q_j(1+x^2)^{-2}$ with $x = \beta_j r$;
- centred on Pt in the anharmonic refinements *A*, *E*, and *F*, $q_{\text{Pt}} \exp(-x^4)\{1-\gamma_{\text{Pt}} P(x)\}$ with *P* a polynomial of $x = \beta_{\text{Pt}} r$, designed for removing positive density near the atomic centre and negative density at $r > 0.35$ Å;
- centred on Pt in the deformation-density refinements *B*, *C*, and *D*, a similar function designed for removing positive density around Pt for $r < 0.6$ Å.

The coefficients c_{Pt}, q_{Pt}, q_{K}, q_{Cl}, β_{Pt}, β_{K}, β_{Cl}, and γ_{Pt} were fitted by least squares to the difference maps.

The residual map of Fig. 3 shows that the anharmonic refinement *A* parametrizes well the features of Fig. 2 at K and Cl, which now appear on the corresponding difference map. However, model *A* cannot account for all the features at Pt; both the residual map and the difference map show maxima on [111], but at different distances from the centre.

In contrast, both charge density refinements *B* and *C* (Figs. 4 and 5) are unable to parametrize the electron densities at any of the atoms. It appears that the residual map becomes flat only for atoms with two adjustable radial exponents α as evidenced by Fig. 6 representing refinement *D* (remember that for reasons of convergence, Pt was attributed only one α and correspondingly shows the same features as on Figure 5). However, compared to refinement *S*, Cl is now displaced by 0.02 Å away from Pt and U_{par} decreases by a factor of 3 (Table 1): the flat residual map at Cl has been obtained at the price of large shifts of the standard parameters. Thus, although *D* is a successful model for K and Cl, it may not be physically meaningful. The difference maps of Figs. 4 to 6 show important densities off the bond axis at Cl, which differ strongly from those of Figure 2. This effect is related to the spherical density subtracted at Cl in these maps (not shown explicitly), which is much larger and sharper than the one subtracted to obtain Figs. 3, 7, and 8.

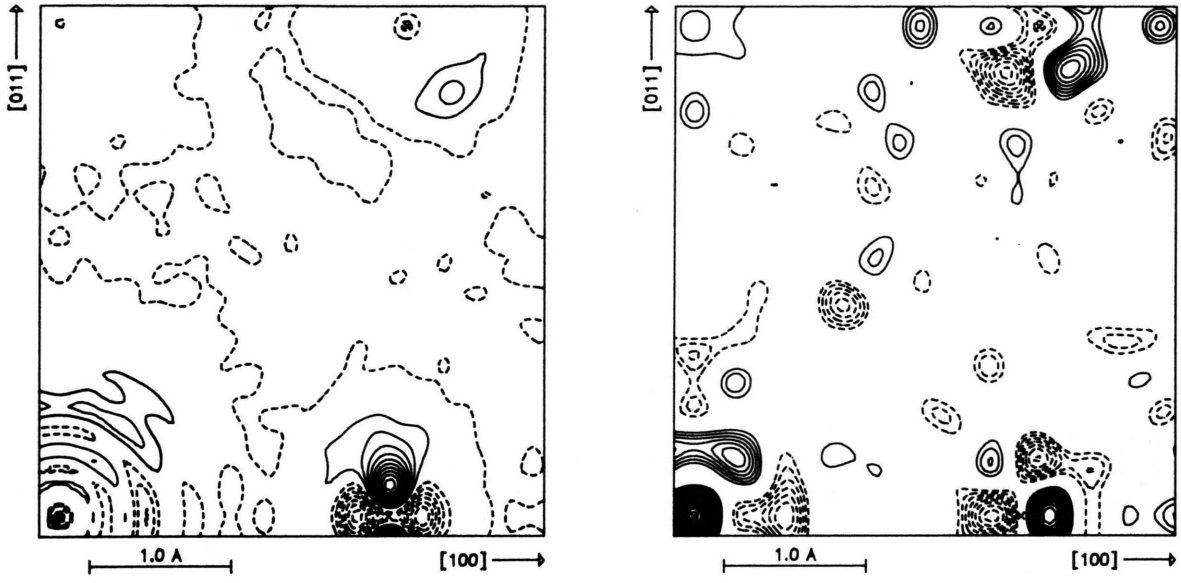

Fig. 4. Difference map (left) and residual map (right) of the deformation density refinement *B*. Intervals as in Figure 3.

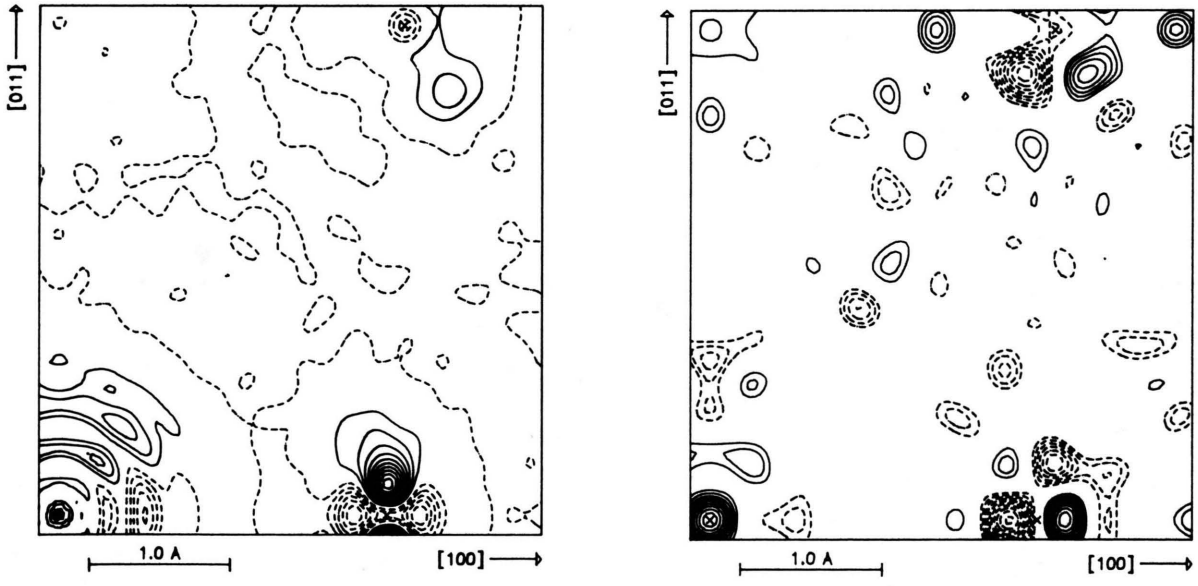

Fig. 5. Difference map (left) and residual map (right) of the deformation density refinement *C*. Intervals as in Figure 3.

The combined anharmonic and deformation-density models *E* and *F* (Figs. 7 and 8) are both successful in accounting for all the residual densities of *S*. They differ in the way they attribute the densities, and in particular the monopoles, to anharmonicity or chemical bonding. The main disagreement of the difference maps of *E* and *F* is near the centre of Pt. In fact, *E* seems to disagree with most of the maps and in particular with *A* (Fig. 3) in showing a minimum on [111] and a maximum on [100].

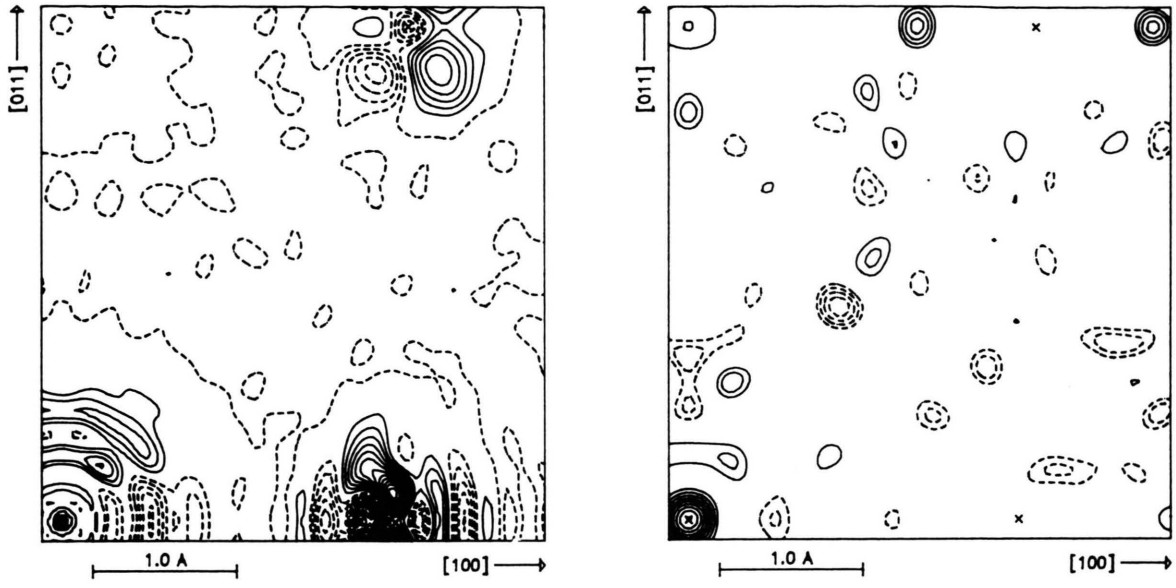

Fig. 6. Difference map (left) and residual map (right) of the deformation density refinement *D*. Intervals as in Figure 3.

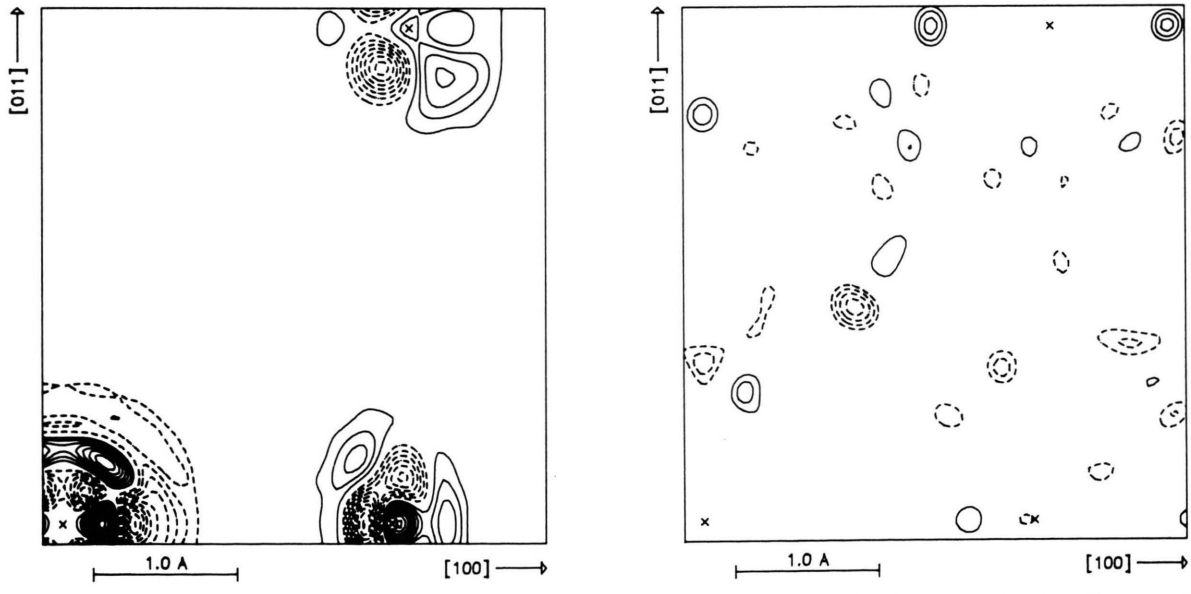

Fig. 7. Difference map (left) and residual map (right) of the combined anharmonic and deformation density refinement *E*. Intervals as in Figure 3.

Conclusions

All the models resulting in flat residual maps produce approximately the same total electron density; small differences follow only from somewhat different F_c-values. However, the models imply very different physical interpretations, i.e. densities are attributed in different ways to thermal motion and to bonding. It is evident that the Hirshfeld model *B* is unsuccessful at all atomic sites, and that the thermal displacement

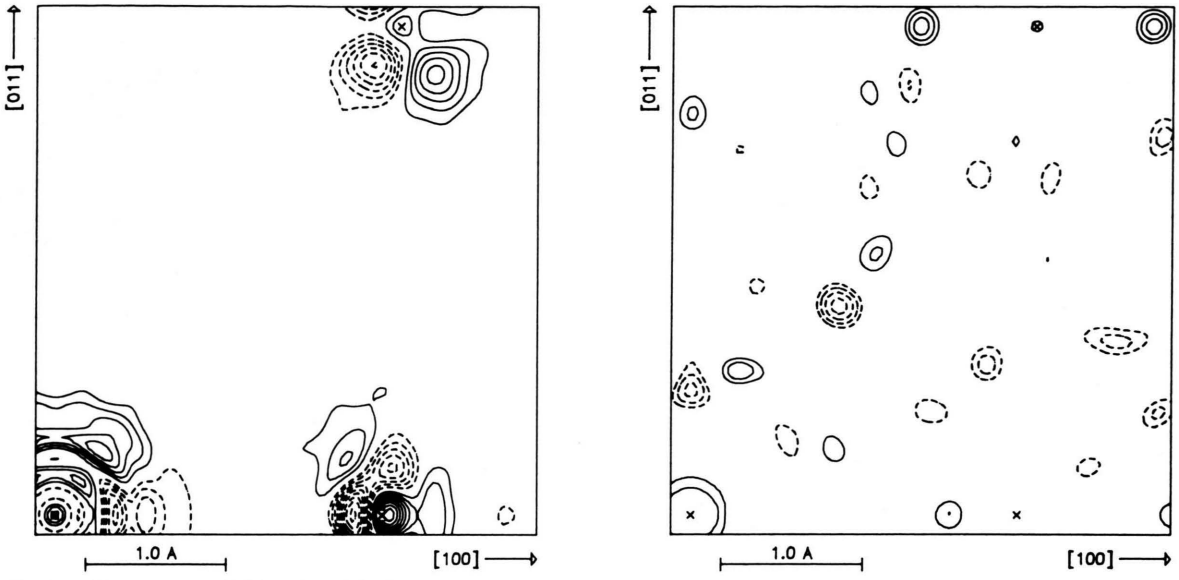

Fig. 8. Difference map (left) and residual map (right) of the combined anharmonic and deformation density refinement *F*. Intervals as in Figure 3.

model *A* is unsuccessful at Pt, indicating the need for a very flexible model such as *E* or *F*.

In the absence of additional information, we may prefer the models with fewest adjustable parameters. *F* may also be preferred to *E*, since the values of the standard parameters of *F* agree somewhat better with those of *S*. Refinement *A* then indicates that K and Cl are undergoing anharmonic displacements with larger amplitudes towards the unoccupied Cl_6-octahedron and smaller amplitudes towards the neighbouring Pt (Fig. 1), in agreement with qualitative expectations. The anharmonicity shift of Cl is 0.0023 Å towards Pt. For Pt, the peaks at distances of 0.29 and 0.55 Å on [111] (Fig. 8) indicate anharmonic displacements as well as preferentially occupied 5d-orbitals with t_{2g}-symmetry.

In their low-temperature study (120 K, $(\sin\theta/\lambda)_{max} = 1.15\,Å^{-1}$), Takazawa, Ohba and Saito [5] found maxima of both the experimental and theoretical deformation density on ⟨111⟩ at distances of about 0.5 Å from Pt. Surprisingly, they were unable to parametrize these maxima with an anharmonic displacement model. Their experimental map shows a maximum near Cl, as does ours, but at a somewhat larger distance from the atom centre. In addition, they do not report a spherically-symmetric accumulation of density on Pt. The region of K is not included in their maps. We have no ready explanation for the disagreement with our results. As far as we can judge, our data set does not seem to be of inferior quality: the internal *R*-value of symmetry-equivalent intensities is lower, the $\sin\theta/\lambda$-limit is higher and, as reported above, the measured crystal shape agrees perfectly with the unaveraged intensity observations.

Maslen [15] has presented a Fourier difference map of isostructural K_2SiF_6 showing features at K in very good agreement with our results. His map also shows a low maximum near F whose position agrees with the maximum we find near Cl.

Clearly, a more direct determination of anharmonicity in K_2PtCl_6 would give valuable information concerning the applicability of widely used crystallographic charge density and thermal displacement models to heavy-atom compounds. Since it is presently difficult to obtain single-crystal neutron data of resolution and accuracy comparable to our present X-ray data, we plan to collect an accurate low-temperature X-ray data set in the near future.

We gratefully acknowledge the support of Prof. Yao Xin-Kan, Nankai University, Tianjin, Peoples Republic of China. This project is supported by the Swiss National Science Foundation.

[1] F. L. Hirshfeld, Isr. J. Chem. **16,** 168 (1977).
[2] K. Toriumi and Y. Saito, Adv. Inorg. Chem. Radiochem. **27,** 27 (1983).
[3] R. Restori and D. Schwarzenbach, Acta Cryst. B **42,** 201 (1986).
[4] E. Nowack, D. Schwarzenbach, and Th. Hahn, Acta Cryst. B **47,** 650 (1991).
[5] H. Takazawa, S. Ohba, and Y. Saito, Acta Cryst. B **46,** 166 (1990).
[6] P. J. Becker and P. Coppens, Acta Cryst. A **30,** 129 (1974); Acta Cryst. A **31,** 417 (1975).
[7] C. K. Johnson and H. A. Levy, in: International Tables for X-Ray Crystallography, Vol. IV, present distributor D. Reidel, Dordrecht 1974, p. 314.
[8] R. F. Stewart, Acta Cryst. A **32,** 565 (1976).
[9] F. L. Hirshfeld, Isr. J. Chem. **16,** 226 (1977).
[10] K. Kurki-Suonio, Isr. J. Chem. **16,** 115 (1977).
[11] D. Schwarzenbach and H. D. Flack, Acta Cryst. A **47,** 134 (1991).
[12] International Tables for X-Ray Crystallography, Vol. IV, present distributor D. Reidel, Dordrecht 1974, p. 99, 149.
[13] D. Schwarzenbach, in: Crystallographic Computing 5: From Chemistry to Biology (D. Moras, A. D. Podjarny, and J. C. Thierry, eds.), Oxford University Press (1991), pp. 69–78.
[14] E. Blanc, D. Schwarzenbach, and H. D. Flack, J. Appl. Cryst. **24,** 1035 (1991).
[15] E. N. Maslen, in: Collected Abstracts (M. Springborg, A. Saenz, and W. Weyrich, eds.), Sagamore X Conference on Charge, Spin and Momentum Densities, Konstanz 1991, pp. 79–80.